

Imaging fast processes in liquid metal foams and semi-solid alloys using synchrotron radioscopy with spatio-temporal micro-resolution

S. Zabler* (a, d), A. Rack (b, c), F. García-Moreno (d), A. Ershov (c), T. Baumbach (c), J. Banhart (d)

(a) Technische Universität Berlin, Institut für Werkstofftechnik, Strasse des 17. Juni 135/ EB 13, 10623 Berlin, Germany. Simon.zabler@tu-berlin.de , *) corresponding author

(b) European Synchrotron Radiation Facility, BP 220, 38043 Grenoble Cedex, France

(c) Forschungszentrum Karlsruhe GmbH – ANKA, Hermann-von-Helmholtz Platz 1, 76637 Karlsruhe, Germany

(d) Helmholtz-Zentrum Berlin, Institute of Applied Materials, Glienicker Str. 100, 14109 Berlin, Germany

Abstract: New x-ray sources of unmatched brilliance, like the superconducting undulator device at ESRF high-energy beamline ID15A, allow for micro-radioscopic investigations with time-resolution up to the micro-second range. Here we present first results of two recent in-situ experiments: the visualization of semi-solid metal flow at an acquisition speed 500 frames/second (fps) and the collapse of pore walls in liquid metallic foams investigated at 40 000 fps. Both applications reveal important qualitative and quantitative facts about the dynamic processes in liquid and/ or semi-solid metals which were inaccessible until now because of either the limited spatial and / or the limited time-resolution of conventional x-ray devices. Thus, semi-solid slurry is observed to break into small particle clusters when injected at high speed. The event of cell wall collapse in metal foams is found to take ~1-2 ms time, indicating that the dynamics of this system is inertia controlled.

Keywords: Synchrotron radiation, x-ray imaging, high-speed radioscopy, metal foams, semi-solid metals, flow analysis, pore coalescence.

Introduction

The outstanding scientific value of time resolved imaging is known since the famous high-speed movies of living insects by Lucien Bull [1]. Yet, time-resolved x-ray imaging of metals was not considered until the construction of the first hard x-ray synchrotron sources. Metallic objects are opaque to visible light. Thus, only microscopy of cut and polished surfaces provides an insight into their bulk microstructure, a method which sacrifices the object under investigation. For non-destructive imaging the use of x-rays is mandatory, particularly when liquid metals are under investigation as it is the case in industrial processing and forming of light metallic components which take place at high temperatures [2]. Metal-foaming (MF) as well as semi-solid casting (SSC) of aluminum alloys represent two of the most advanced processing routes for the production of light functional materials [3,4].

Casting of metal alloys which are only partially molten reduces costs and unwanted volume shrinkage due to the lower processing temperature. Up to now, SSC suffers from the incomplete understanding of the rheological properties of this two-phase mixture which is necessary for numerical simulation and optimization of the process [5,6]. Particularly for thin cavities of dimensions which are similar to the average particle/ cluster size of the solid-phase, SSC yields only poor results. In situ radioscopy now provides a tool for visualizing the injection process directly [7].

A large number of processing routes exist for metal foams. The one which is investigated here employs powder-compacted metallic precursors mixed with TiH_2 particles, the so called “blowing agent”. When heated to a certain temperature (which is slightly above the melting point of aluminum) the particles decompose, setting free hydrogen which forms gas bubbles separated by liquid melt. An inhomogeneous size distribution of pores and particularly the formation of large pores by growth and coalescence can cause problems for the mechanical stability of the structure and thus, have to be avoided [4]. Again, in situ x-ray images provide the key to understand the dynamics of pore coalescence in MF [8].

Although their spatial resolution has improved over the past decades, commercial radioscopy devices lack the sufficient time-resolution to study the above mentioned processes [2,9]. Unlike x-ray tubes, synchrotron sources provide an extremely high brilliance allowing for fast micro-radioscopy: i.e. the possibility to image the internal structure of an object with micrometer resolution can be extended to study its temporal evolution as well. Here we present results from high-speed radioscopy on liquid metal foams and injection of semi-solid metals performed at ESRF's “*High Energy Diffraction and Scattering Beamline*” ID15A [10].

Materials and Method

1. Semi-solid injection

An experimental setup for in situ flow monitoring of semi-solid slurry was constructed by the Helmholtz-Zentrum Berlin and the Federal Institute for Materials Research and Testing (BAM), both Germany. This setup is detailed in Fig. 1.

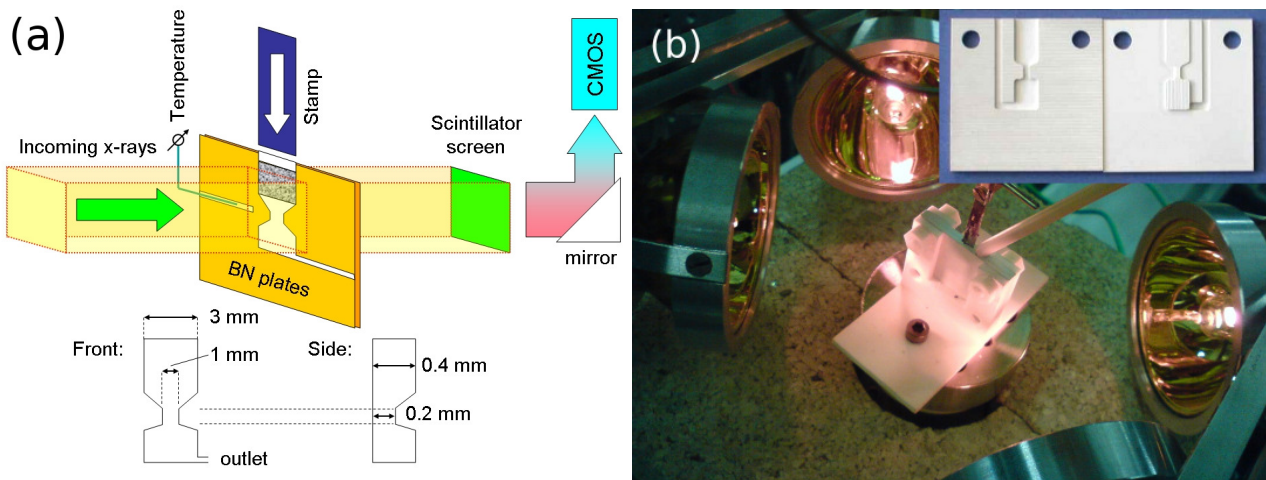


Figure 1: (a) Schematic drawing of the in-situ radiography setup for measuring semi-solid metal flow. (b) Photo of the semi-solid experiment: Four heating lamps point towards the sample chamber which is machined into two Boron-Nitride (BN) plates (inset) which are fixed in a ceramic holder. The thin steel piston which is used for the injection enters the cavity from above, right next to the thermocouple which is shielded by a ceramic tube.

At the beginning of the experiment a small piece (3 mm x 3 mm x 0.4 mm) of grain refined Al-Ge32 alloy (including 4% AlTiB5 grain refiner – AFM Affilips, Netherlands) was inserted into a flat injection reservoir between two 1 mm thick boron nitride (BN) plates. Instead of using the alloy Al-Si7(wt.%) - which is commonly used for SSC - we employed Al-Ge32 which has similar solid and liquid volume fractions but provides - unlike Al-Si7 - sufficient x-ray density contrast between the two phases. Concerning solid volume fraction and crystal structure, Al-Ge32 is also very similar to Al-Si7. Similar to the binary Al-Si system, Al-Ge features a simple eutectic phase diagram with two two-phase regions in the semi-solid state. At 450°C, the temperature where the experiment took place, solid and liquid volume fractions are 0.49 and 0.51, respectively. Average size of the solid Al-particles was 50 - 70 μm in diameter as estimated from microscopy images of polished sections. BN was used because of its high melting point and low x-ray absorption. Furthermore, BN does not react with the liquid Al-Ge melt.

A specific channel-geometry was used for the semi-solid flow-experiment. A bottleneck-shaped flat channel was machined into a pair of BN-plates, reducing the effective cross-section to 1 mm x 0.4 mm. Further below this ~2 mm long bottleneck, there is a recipient of the same dimensions as the reservoir at the top, with a small gas outlet to the side. The BN plates are clamped between two U-shaped ceramic supports and the whole setup is positioned such that the metallic sheet is facing the

incoming X-ray beam. For heating the sample, we used four Osram Xenophot 64635 HLX (150 W) heating lamps, positioned obliquely with respect to the BN plates faces which were slightly moved out of the lamps' focus to achieve uniform heating.

After heating the mould and the alloy to 450°C, the injection was performed by driving a steel piston into the mould, thus pushing the semi-solid slurry through the bottleneck. The piston was driven at a speed of $v = 2$ cm/s using a linear stepping motor. Images were acquired at 500 fps and ~ 9 μm effective pixel size. Since the readout time of the CMOS camera is negligibly short, each frame corresponds to an exposure of 2 ms.

2. Metal foaming

Foamable aluminum precursors were prepared according to the powder metallurgical route, i.e. by mixing the elemental metal powders with TiH_2 acting as foaming agent and consolidating these. The precursors were foamed inside a furnace pressurized with argon gas. The furnace comprises an AlMg tube (40 mm diameter and 0.5 mm wall thickness) with a ceramic heating plate. The setup has already been described in more detail by García-Moreno et al. [11]. The coalescence rate during foaming under normal conditions is usually in the range of some events per second in a sample of the size used. To accelerate expansion during the short available time window (a few seconds) and to provide more observable coalescence events, we depressurized the furnace during expansion. Owing to fast expansion of the foam during pressure release, a large number of coalescence events could be recorded. Recent experiments showed that frame rates above 10 000 fps are required in order to temporally resolve a single cell wall collapse [12].

In summary, the foaming procedure comprised three steps: (i) heating of the precursor under 5 bar pressure, (ii) melting of the precursor and nucleating pores still under pressure, and (iii) fast pressure release from 5 bar to 1 bar, thereby triggering fast foam expansion.

3. High-speed micro-radioscopy

Experiments with white synchrotron radiation were carried out at the beamline ID15A of the European Synchrotron Radiation Facility (ESRF), France [10]. Radiographic images are recorded via a scintillator screen which converts x-ray photons into visible light. The resulting luminescence image is magnified onto a high-speed CMOS camera using diffraction limited visible light optics. For high-speed data acquisition the Photron Fastcam SA-1 CMOS camera with 10-bit dynamic range was used [13]. The camera can record 5400 fps in full-frame mode (1024×1024 pixels) and up to 675000 FPS when using a region of interest (ROI). The shortest shutter time is 2 μs ; triggering at 100 ns time resolution. Images are first stored in the 32 Gbyte onboard memory (which defines the maximum recording length) and then are transferred to a computer. A magnification of 2.5 was used for the semi-solid experiment, whereas for the metal foaming experiment, the optical

system was designed to yield a 1:1 projection onto the camera [14]. As scintillating material, commercially available bulk LuAG:Ce (200 μm thick) was chosen which is known to be suited for fast synchrotron-based imaging involving high heat loads [10]. The soft x-radiation was filtered with 25 mm silicon, leading to an X-ray photon flux density in the range of 10^{15} photons. s^{-1} . mm^{-2} .

Results

1. Semi-solid flow

Figure 2 displays four radiographs showing the injection into the bottleneck-channel (a-d): The pictures were taken in time-intervals of 100 frames (0.2 s) each of them showing an exposure of 2 ms. The gray values show the negative logarithm of the normalized intensity $-\ln(I/I_0) \sim \Sigma\mu \cdot d$ with μ the linear x-ray absorption coefficient and d the thickness of the material. After subtraction of the detector dark current the radiographs are normalized with flatfield images I_0 .

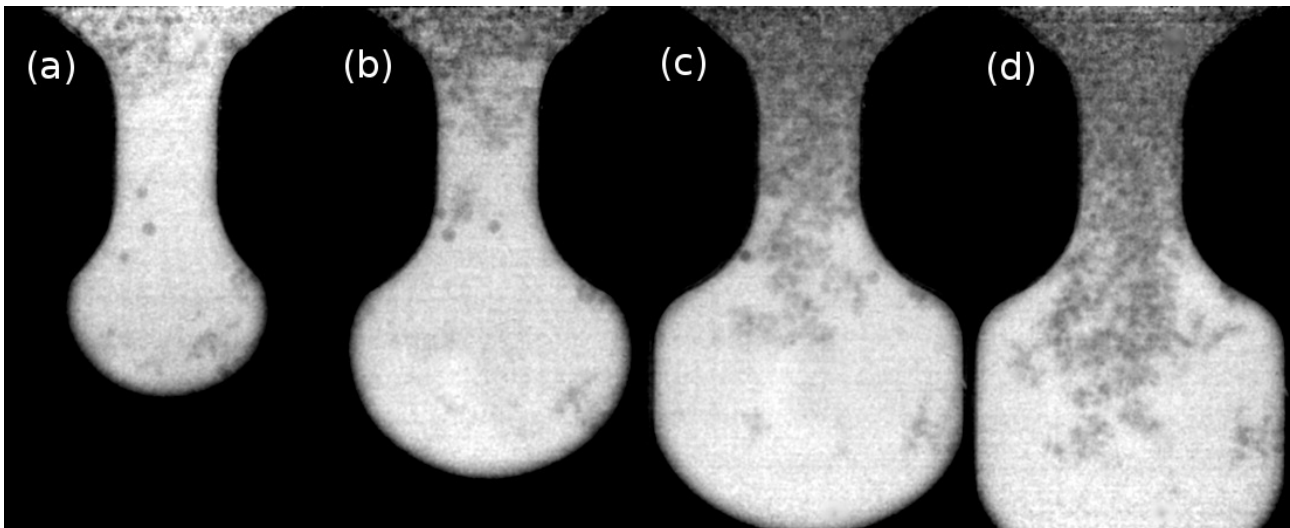


Figure 2: Selected radiographs representing time-intervals of 0.2 s, each image corresponding to an exposure of 2 ms. (a) After starting the semi-solid injection, first the liquid phase traverses the bottleneck channel and flows into the recipient below. Some particles can be seen at the air-liquid interface. Round dark isolated objects were identified as gas bubbles. (b) First particle clusters detach from the solid matrix and traverse the channel. (c) The bottleneck is completely filled with solid phase, some clusters reaching into the recipient. (d) End of the injection: The remaining solid (top) is compacted whereas the recipient is only partially filled.

Since the sample thickness is constant Fig. 2 basically shows a density / atomic number contrast between three phases: air (black), liquid melt (bright gray) and solid particles (dark gray). First, we observe the liquid melt entering the channel and filling the recipient. Meanwhile solid particles and particle clusters detach from the solid skeleton and follow the liquid flow at high speed into the cavity. Few particles/ clusters stay very close to the liquid-air interface whereas most particles which traverse the bottleneck are moving through the liquid. During the experiment small air bubbles appear in the liquid as black spherical objects and disappear soon after their emergence

possibly due to dissolution of the gases in the melt. With the recipient filled with liquid and some solid particles / clusters and the flow coming to a halt, the remaining solid feedstock can no longer traverse the channel and the down-driving piston is seen to compact the particles to a dense aluminum-rich matrix (top of Fig. 2d).

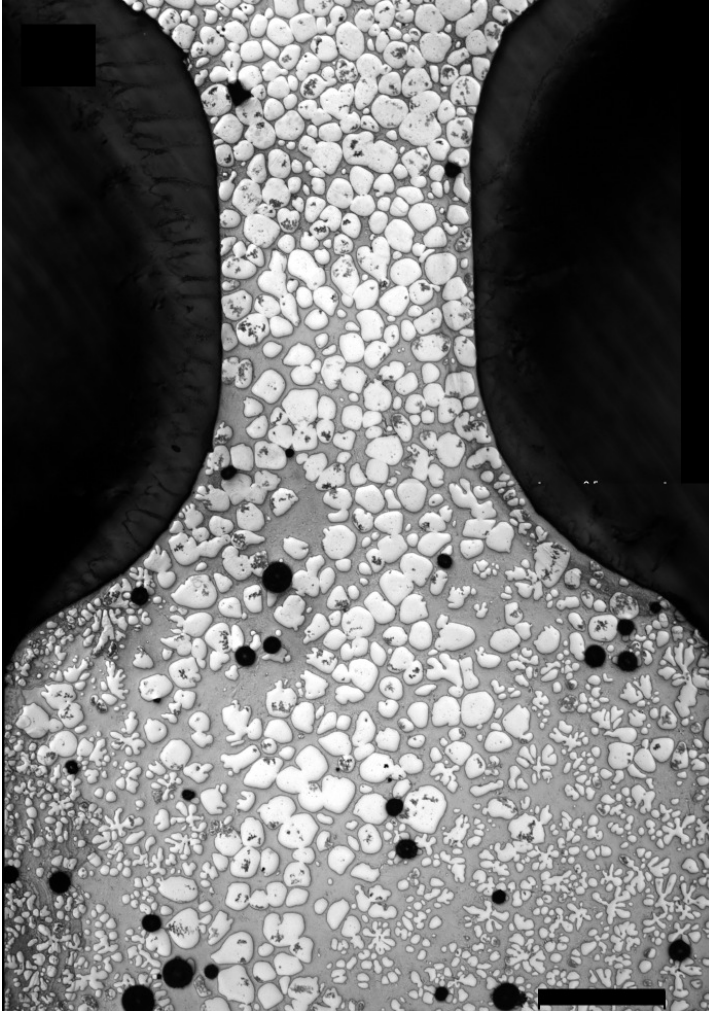


Figure 3: Metallographic section prepared from the recovered material after the synchrotron experiments showing a magnified view of the metallic microstructure in a bottleneck cavity (bar equals 0.5 mm).

After each experiment the heating lamps were switched off allowing the alloy to cool down. Metallographic cuts were prepared from the cold samples in order to compare the polished sections with the high-temperature radiographs. The section for the geometry shown previously is depicted in Fig. 3. The microstructure is in agreement with the radiosopic observations. Aluminum particles at the channel entry (top) appear compressed by the piston. Particles inside the bottleneck channel feature a globular shape whereas the former liquid phase in the recipient now consists of dendrite aluminum precipitates (created during the cooling from 450°C down to 420°C) and the surrounding eutectic material (which solidified at the eutectic temperature 420°C).

First quantitative results calculated from the radiograph in Fig. 2c are shown in Fig. 4. We used optical flow analysis to calculate the two-dimensional displacements between two consecutive x-ray images. The method is based on the classical approach proposed by [15] and determines the

unknown displacement field as the minimization of a suitable energy functional [16].

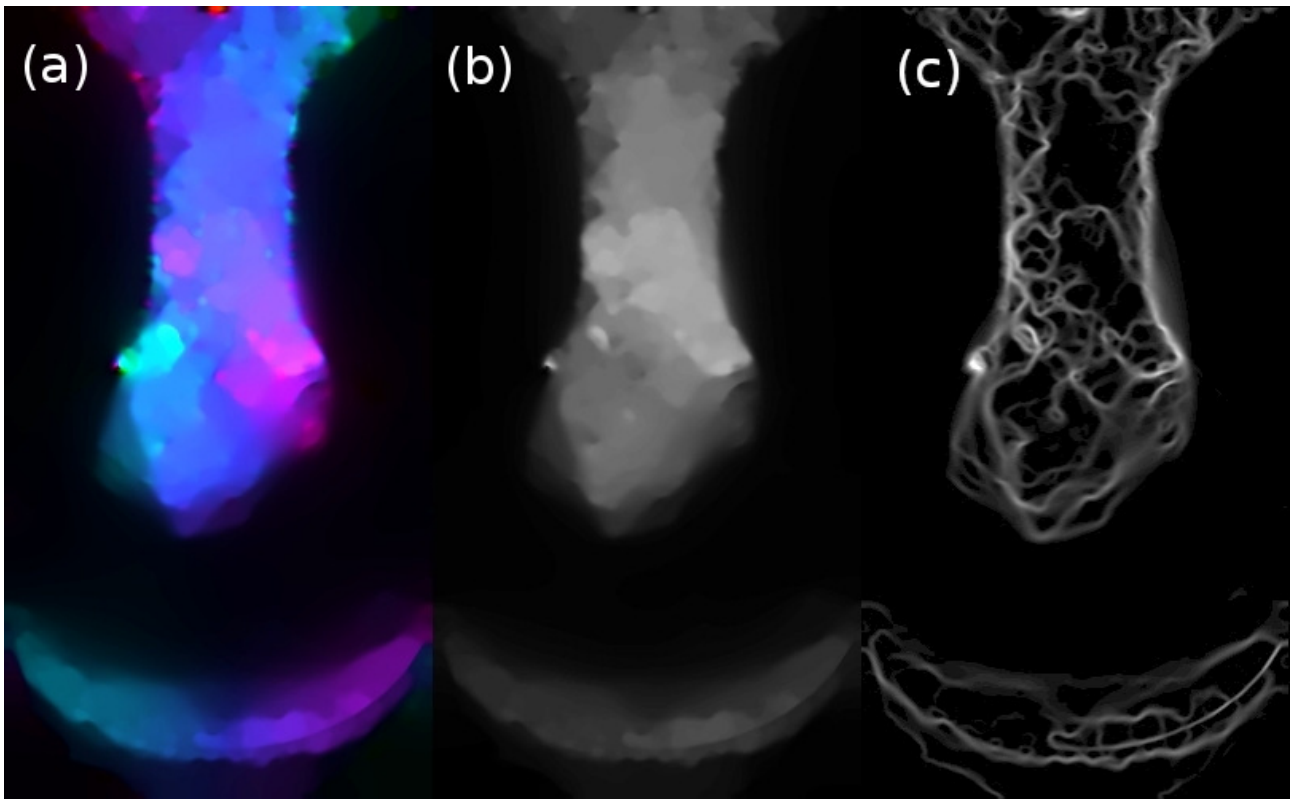


Figure 4: Optical flow analysis of semi-solid motion corresponding to the radiograph shown in Fig. 2c. (a) Optical flow map: Color represents flow direction; Brightness represents the flow amplitude which is shown in (b). (c) Velocity gradient map calculated from (a) indicating the coercive motion of larger particle clusters.

Such an energy functional comprises two terms, which impose constancy on specific image features and assumes that the optical flow field varies smoothly. Figure 4a shows the flow field using the color pseudo-coding whereby color represents the direction and brightness is scaled with the displacement amplitude (shown in gray values in Fig. 4b). Two types of motion can be detected with this method: i. Motion of the liquid-air interface and ii. motion of solid particles / clusters. Indeed, the velocity gradient which is shown in Fig. 4c indicates that solid particles move in larger clusters / grains.

2. Metal foaming

Figure 5 displays an image sequence taken during metal foaming of an aluminum precursor. The radiographs were acquired at ultra-high speed (40 000 fps), each frame representing 25 μs of exposure. With this spatio-temporal micro-resolution we were able to picture the collapse of a single cell wall including the relaxation of the novel pore. The time sequence shown in Fig. 5 lasted over 1.7 ms and major events are sketched with the original image faded into the background below the radiographs. Figure 5a shows the two neighboring pores, 525 μs later (Fig. 5b) the cell wall collapse starts. Relaxation (Fig. 5c) takes place until finally a mechanically stable, new round cell

wall forms after a total time of 1700 μs (Fig. 5d) [17]. For watching the full movie, please see [18].

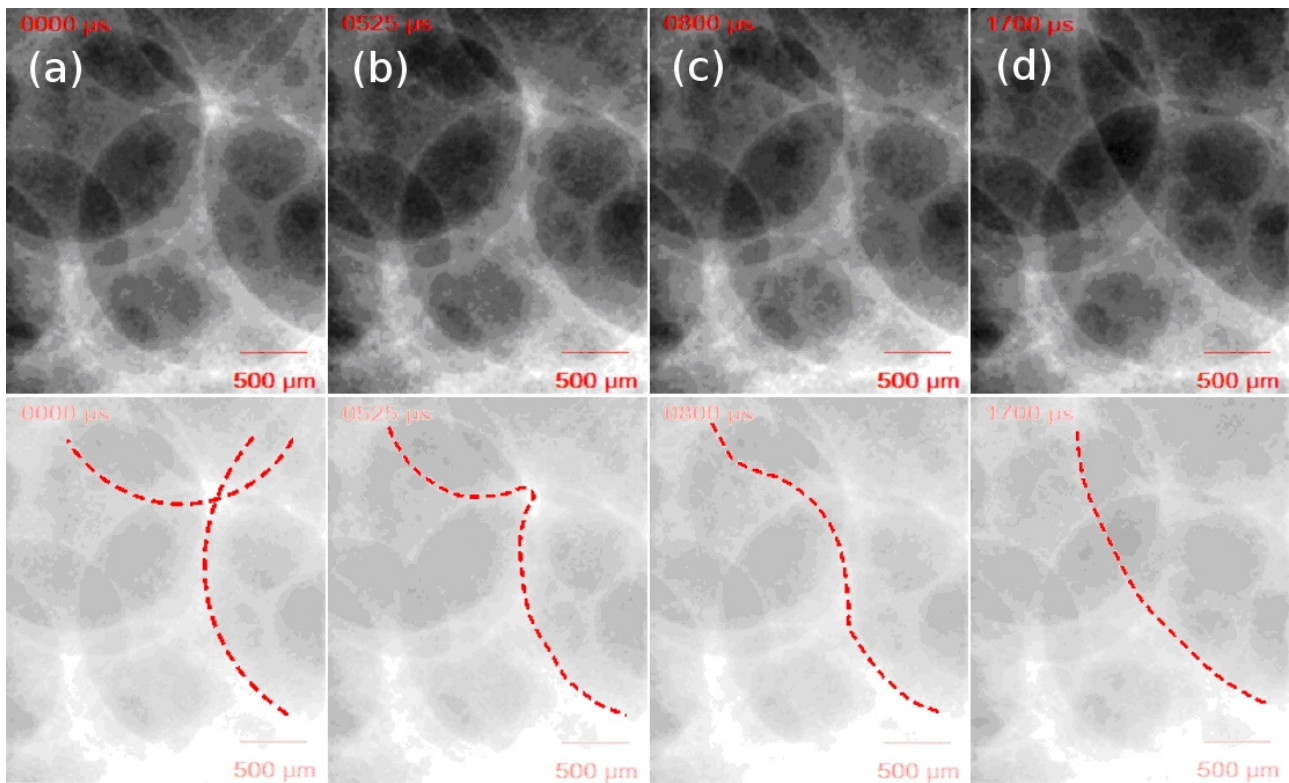


Figure 5: Application of ultra-high-speed radioscopy (40 000 fps) to visualize the single cell wall collapse in liquid aluminium foam. The complete event takes place ~ 1.7 ms, each frame represents 25 μs exposure [17].

Discussion

By imaging the injection of semi-solid aluminum alloy into recipients we could visualize the flow dynamics of this two-phase system both qualitatively and quantitatively, to a level where we are close to tracing the motion of individual solid particles / clusters through the liquid melt. Radioscopy further revealed how the problem of inhomogeneous microstructures in thin-walled semi-solid cast components arises due to limited penetration-ability of larger solid particles / clusters and compaction of the solid skeleton at bottlenecks and corners. By using a 1:1 imaging system (pixel size 20 μm) and by applying a ROI for the CMOS chip to a smaller box we captured the collapse of individual cell walls during foaming of a liquid aluminum. Qualitative assessment of the data showed that the total collapsing event takes slightly longer than one millisecond.

Note that due to the necessary application of strong absorption filters (to limit heat load for the detector screen) we used only a small portion of ID 15A's full photon flux. The resulting high energy spectrum further produced absorption values of $\mu.t \sim 0.4-0.5$, in other words the signal-to-noise ratio of such experiments can improve dramatically when the experiment is moved to lower-energy beamlines, thus producing values closer to $\mu.t \sim 2.2$ which is the theoretical optimum for x-ray imaging [19].

Conclusions

We presented first results obtained from the combination of white synchrotron radiation with CMOS cameras on indirect X-ray pixel detectors. We proved that it is possible to acquire x-ray movies with a spatio-temporal resolution up to the micro-scale. We believe that synchrotron based high-speed and ultra-high-speed radioscopy have the potential to reveal new outstanding dynamics in a large variety of systems. Particularly the dynamics of liquid and / or semi-solid metals cannot be visualized by any other technique and they do require these high frame rates to produce experimental data which is comparable to numerical flow- and / or foaming FE simulations that are designed to mimic and optimize industrial processes of critical importance.

Acknowledgements

We thank T. Martin, C. Jarnias, M. Peele, M. Di Michiel, V. Honkimäki, T. Weitkamp (ESRF), A. Dieterich, L. Körner (Universität Tübingen), D. Haas, A. Cecilia, T. Rack, H. Schade, A. Volker (ANKA), N. Kardjilov, A. Hilger and G. Choinka (Helmholtz-Zentrum Berlin) for support and fruitful discussions. H. Kropf and C. Förster for the metallographic work. W. Tutsch (PCO AG, Germany) and A. Bridges (Photron Inc., USA) enlightened us about CMOS cameras. Our gratitude further goes to M. Klinger, H. Heimbach and H. Riesemeier from the Federal Institute for Material Testing Berlin (BAM, Germany) for constructing and building the semi-solid experimental setup.

References

1. L. Bull (1928) *La Cinématographie*; Paris: Armand Collin.
2. S. Boden, S. Eckert, B. Willers and G. Gerbeth (2008) X-Ray Radioscopic Visualization of the Solutal Convection during Solidification of a Ga-30 Wt Pct In Alloy, *Metall. Trans. A* 39A: 613–23.
3. M. C. Flemings (1991) Behavior of metal alloys in the semisolid state, *Metall. Trans. A* 22A: 957–81.
4. C. J. Yu, H. Eifert, J. Banhart, J. Baumeister (1998) Metal foaming by a powder metallurgy method: Production, properties and applications, *Mat. Res. Innovat.* 2: 181-188.
5. F. Ilinca, J.-F. Héту, J.-F. Moisan and F. Ajersch (2008) Three-dimensional injection molding simulation of AZ91D semi-solid magnesium alloy, *Int. J. Mater. Form.* 1: 3–12.
6. M. Hufschmidt, M. Modigell and J. Petera (2006) Modelling and simulation of forming processes of metallic suspensions under non-isothermal conditions, *J. Non-Newtonian Fluid Mech.* 134: 16–26.
7. S. Zabler, A. Rack, A. Rueda, L. Helfen, F. Garcia-Moreno, J. Banhart (2009) Direct observation of particle flow in semi-solid alloys by synchrotron X-ray micro-radioscopy, *Phys. Stat. Solid. A* 207(3): 718-723.
8. A. Rack, F. García Moreno, T. Baumbach, J. Banhart (2009) Synchrotron-based radioscopy employing spatio-temporal micro-resolution for studying fast phenomena in liquid metal foams, *J. Synchrotron*

Rad. 16: 432-434.

9. J. N. Koster, T. Seidel, R. Derebail (1997) A radiosopic technique to study convective fluid dynamics in opaque liquid metals, *J. Fluid Mech.* 343: 29–41.
10. M. Di Michiel, J. M. Merino, D. Fernandez-Carreiras, T. Buslaps, V. Honkimäki, P. Falus, T. Martins, O. Svensson (2005) Fast microtomography using high energy synchrotron radiation, *Rev. Sci. Instrum.* 76: 043702.
11. F. García-Moreno, N. Babcsan, J. Banhart (2005) X-ray radioscopy of liquid metalfoams: influence of heating profile, atmosphere and pressure, *Colloids Surf. A* 263(1-3): 290-294.
12. F. García-Moreno, A. Rack, L. Helfen, T. Baumbach, S. Zabler, N. Babcsan, J. Banhart, T. Martin, C. Ponchut, M. Di Michel (2008) Fast processes in liquid metal foams investigated by high-speed synchrotron x-ray microradioscopy, *Appl. Phys. Lett.* 92(13): 134104-1 – 134104-3.
13. T. Inoue, S. Takeuchi, S. Kawahito (2005) CMOS active pixel image sensor with in-pixel CDS for high-speed cameras, *Proc. of SPIE* 5580: 293-300.
14. A. Koch (1994) Lens coupled scintillating screen-CCD X-ray area detector with a high quantum efficiency, *Nucl. Instr. & Meth. in Phys. Res. A* 348: 654-658.
15. B. Horn and B. Schunck (1981) Determining optical flow, *Artificial Intelligence* 17:185–203.
16. T. Brox, A. Bruhn, N. Papenberg, J. Weickert (2004) High accuracy optical flow estimation based on a theory for warping, in T. Pajdla and J. Matas (eds.), *Computer Vision – ECCV 2004 of Lecture Notes in Computer Science* 3024: 25–36. Springer, Berlin.
17. A. Rack, F. García-Moreno, O. Betz, S. Zabler, C. Schmidt, T. dos Santos Rolo, A. Ershov, T. Rack, L. Helfen, J. Banhart, T. Baumbach (2008) Synchrotron-based radioscopy with spatio-temporal micro-resolution using hard X-rays, *IEEE Nucl. Sci. Symp. Conf. Rec. (NSS '08)*: 528-531
18. http://www.alexanderrack.eu/ieee_movie.avi - (last visit 2009)
19. W. Graeff, K. Engelke (1991) Microradiography and microtomography, in S. Ebashi, M. Koch and E. Rubenstein (eds.), *Handbook on Synchrotron Radiation* 4, 361–405. Elsevier Science Publishers B.V., Swansea.